Recent crustal deformation in west-central South America

Thesis by

Matthew E. Pritchard

In Partial Fulfillment of the Requirements

for the Degree of

Doctor of Philosophy

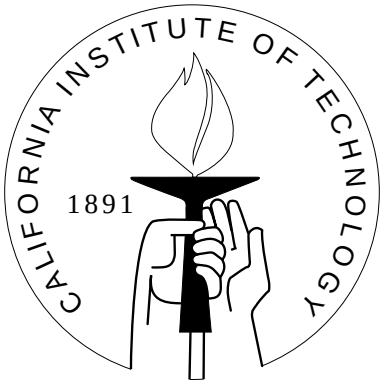

California Institute of Technology

Pasadena, California

2003

(Submitted 5/12/2003)

Acknowledgements

My 6 years at Caltech have been very rewarding, and I am glad for the opportunity to thank some of those responsible. First, I thank Dave Stevenson for convincing me to come to Caltech, for many enlightening discussions, and serving as a role model for presenting material clearly. I owe much to my advisor, Mark Simons, whose generosity and never-ending fountain of ideas and enthusiasm kept me motivated both in my research and in remote field locations. The faculty and staff in the Seismo Lab, in planetary science, and in the rest of the Division, create a stimulating and welcoming environment – from interactions at Coffee Break to invitations to their homes. The comments (and classes) of committee members Hiroo Kanamori and Mike Gurnis are especially appreciated. I thank Rosemary Miller for always keeping a close account of where the money or data shipments were, Mike Black for his computer assistance, and Kimo Yap for his ability to keep so many programs and machines working. Additional thanks to Irma Black, Donna Sackett, Viola Carter, Jim O'Donnell, Susan Leising and Ed Sponsler and the Caltech Electonic Thesis development team for assistance with the electronic appendix

I have greatly benefited from collaboration with many scientists at the Jet Propulsion Laboratory. Simply stated, I would not have been able to overcome some technical hurdles without the assistance of Paul Rosen, whose knowledge and good humor are appreciated. I further acknowledge useful conversations with many of the JPL SAR group: Scott Hensley, Frank Webb, Eric Fielding, Elaine Chapin, Ian Joughin, and Paul Lundgren. I thank Tom Farr and Mike Kobrick for providing access to digital elevation models from the Shuttle Radar Topography Mission. I began an interesting project with Marty Slade and Ray Jurgens mapping the topography of

Venus, and I thank them for teaching me about planetary radar and funding my visit to Arecibo for one of the experiments.

At Caltech, many of my fondest memories will be of time spent in the field – more than three months, and mostly unrelated to this thesis. I thank all of those who led field trips or field camps that I participated in: Brian Wernicke, Bruce Murray, Joe Kirschvink, Jason Saleeby, Tom Ahrens, Lee Silver, Paul Asimow, JoAnn Stock, Rob Clayton and Mark Simons. I am grateful to Jorge Clavero, Steve Sparks, Steve McNutt, Mayel Sunagua, and Jose Naranjo who introduced me personally to some of the Andean volcanoes. The American Geophysical Union funded my participation in a conference in Santiago, Chile. I thank JoAnne Giberson for helping to set up the laptop computer software for many of these outings. I particularly thank Joe Kirschvink who took me (and many others) on a research rafting trip down the Grand Canyon, and Kerry Sieh, who led a great trip to Greece and Turkey funded by the generosity of Caltech alum Mike Scott. Terry Gennaro made sure all of these trips were properly equipped, and I thank him for all his efforts.

Numerous people and institutions contributed to individual chapters. All Chapters: Fellowships from Caltech, NSF and NASA supported my graduate studies, and most of the ERS SAR data was acquired as a Category 1 research project from the European Space Agency. The GMT program was used to create several figures (*Wessel and Smith*, 1998). Chapters 1 and 2: JERS data was provided by the Remote Sensing Technology Center of Japan through research users Akiko Tanaka and Paul Rosen. I thank Rowena Lohman, Yuri Fialko, and Luis Rivera for some modeling software, Shan de Silva for an electronic version of his volcano database, Mike Abrams for help with ASTER data, and Brian Savage for assistance with interpreting the seismic data for the shallow earthquake. Chapter 3: I thank Paul Segall and an anonymous reviewer for critical reviews, Stephan Husen, Pierre Ihmlé, and Luc Ortieb for access to their data, and Dave Sandwell for suggesting use of the satellite clock to help find missing lines. Chapters 4 and 5: I thank my co-authors Chen Ji and Mark Simons, and Tim Melbourne for providing the processed GPS data for Arequipa. Chapter 5: JERS data was provided by the Remote Sensing Technology

Center of Japan through research user Paul Rosen, and Melissa Giovanni supplied relocated aftershocks for the Arequipa earthquake. I thank Paul Rosen and Hiroyuki Nakagawa for processing assistance with the JERS data.

Many people prepared me to survive Caltech. I can only begin to thank my parents, who nurtured my curiosity in many ways from a young age. The rest of my family, particularly my grandmother, brother and great aunt have been very supportive. I thank my (distant) cousin Kurt Grimm (now at UBC), who has been a source of geologic information and advice for nearly 20 years. I was fortunate to have many outstanding science teachers along the way, starting with Roberta Oblak, who taught me science, but also how science is relevant to society. In high school, Ed Moyer took extra time to help me develop a Westinghouse project positing a ring system for Pluto, and Robert H. Brown (now at Arizona) carefully reviewed my work and encouraged my further study. Rene Ong (now at UCLA) and the CASA-BLANCA group at Chicago supervised my senior thesis and introduced me to data analysis and field work (installing cosmic ray detectors). I had very fruitful summer internships with Vicki Hansen at SMU and Walter Kiefer at the LPI.

I have been fortunate to have made many lifelong friends and colleagues among the students and postdocs at Caltech, and although I don't have room to thank all of them here, I particularly thank Zilchbrau conspirators Anthony Toigo, Sarah Stewart, Mark Roulston, Brian Savage, and Mark Richardson. For discussions, useful and otherwise, I thank: Jean-Luc Margot, Magali Billen, Francis Nimmo, Shelley Kenner, Sujoy Mukhopadhyay, Emily Brodsky, Nathan Downey, Liz Johnson, Joe Akins, Edwin Schauble, Jascha Polet, Chris DiCaprio, Shane Byrne, Nicole Smith, Ryan Petterson, Alisa Miller, Alex Song, Elisabeth Nadin, Vala Hjorleifsdottir, Antonin Bouchez, Selene Eltgroth, Ben Weiss, Julie O'Leary, Tanja Bosak, Jane Dmochowski and my officemate Patricia Persaud. I also thank my advisor and Martha House, for their hospitality on many occasions. The support and companionship of Rowena Lohman has been, and continues to be particularly meaningful to me.

Abstract

I use interferometric synthetic aperture radar (InSAR) to create maps of crustal deformation along the coast and within the volcanic arc of central South America. I image deformation associated with six subduction zone earthquakes, four volcanic centers, at least one shallow crustal earthquake, and several salt flats. In addition, I constrain the magnitude and location of post-seismic deformation from the aforementioned subduction zone earthquakes. I combine InSAR observations with data from the Global Positioning System (GPS) and teleseismic data to explore each source of deformation. I use the observations to constrain earthquake and volcanic processes of this subduction zone, including the plumbing system of the volcanoes and the decadal along strike variations in the subduction zone earthquake cycle.

I created interferograms of over 900 volcanoes in the central Andes spanning 1992-2002, and found four areas of deformation. I constrained the temporal variability of the deformation, the depth of the sources of deformation assuming a variety of source geometries and crustal structures, and the possible cause of the deformation. I do not observe deformation associated with eruptions at several volcanoes, and I discuss the possible explanations for this lack of deformation. In addition, I constrain the amount of co-seismic and post-seismic slip on the subduction zone fault interface from the following earthquakes: 1995 M_w 8.1 Antofagasta, Chile; 1996 M_w 7.7 Nazca, Peru; 1998 M_w 7.1 Antofagasta, Chile; and 2001 M_w 8.4 Arequipa, Peru. In northern Chile, I compare the location and magnitude of co-seismic slip from 5 $M_w > 7$ earthquakes during the past 15 years with the post-seismic slip distribution. There is little post-seismic slip from the 1995 and 1996 earthquakes relative to the 2001 event and other recent subduction zone earthquakes.

Contents

Acknowledgements **iii**

Abstract **vi**

Overview **1**

0.1 Introduction to subduction zones 1

0.2 Introduction to radar interferometry 4

0.3 Thesis outline 9

1 An InSAR-based survey of deformation in the central Andes, Part I: Observations of deformation: Volcanoes, salars, eruptions, and shallow earthquake(s)? 12

Abstract **13**

1.1 Introduction 14

1.2 Data used 16

1.3 Field work 22

1.4 Results 22

1.4.1 Deforming volcanoes 28

1.4.1.1 Uturuncu 28

1.4.1.2 Hualca Hualca 29

1.4.1.3 Lazufre 30

1.4.1.4 Cerro Blanco (Robledo) 32

1.4.2 Selected non-detection 32

1.4.2.1 Chiliques 32
1.4.3 Eruptions 33
1.4.3.1 Lascar 33
1.4.3.2 Irruputuncu 40
1.4.3.3 Aracar 40
1.4.3.4 Sabancaya 41
1.4.4 Non-volcanic deformation 42
1.4.4.1 Salars 42
1.4.4.2 A shallow earthquake? 47
1.4.4.3 Post-seismic hydrological activity? 48
1.4.4.4 Sources of speculation 50
1.5 Conclusions 53

2 An InSAR-based survey of deformation in the central Andes, Part II: Modeling the volcanic deformation – sensitivity to source geometry and mass balance in a volcanic arc 57

Abstract 58

2.1 Introduction 59
2.2 Modeling strategy 62
2.3 Results 67
2.3.1 Uturuncu 67
2.3.2 Hualca Hualca 79
2.3.3 Lazufre 84
2.3.4 Cerro Blanco (Robledo) 84
2.3.4.1 Physical cause of subsidence 86
2.4 Mass balance in a volcanic arc 90
2.5 Conclusions 95

3 Co-seismic slip from the July 30, 1995, M_w 8.1 Antofagasta, Chile, earthquake as constrained by InSAR and GPS observations 98

Abstract **99**

3.1 Introduction 101

3.2 Previous work 101

3.3 Data used 105

3.4 Data inversion 111

3.5 Discussion 116

3.5.1 Comparison of the slip model with previous work 118

3.5.2 Comparison with other measurements 124

3.6 Summary 129

4 Co-seismic and post-seismic slip from multiple earthquakes in the northern Chile subduction zone: Joint study using InSAR, GPS, and seismology **133**

Abstract **134**

4.1 Introduction 135

4.2 Data used 137

4.3 Modeling strategy 143

4.4 Results 146

4.4.1 1998 earthquake 146

4.4.2 1995 earthquake 147

4.4.3 InSAR sensitivity to small, deep earthquakes 151

4.4.4 Earthquakes from the 1980's 154

4.4.5 Post-seismic 1995-1996 160

4.4.6 Post-seismic 1995-2000 168

4.5 Discussion 170

5 Comparision of co-seismic and post-seismic slip from the November 12, 1996, M_w 7.7 and the June 23, 2001, M_w 8.4 southern Peru subduction zone earthquakes **175**

Abstract **176**

5.1 Introduction 177

5.2 Previous work 179

5.3 Data used 180

5.4 Modeling strategy 183

5.5 Results 186

5.5.1 1996 earthquake 186

5.5.2 2001 earthquake 190

5.5.3 Post-seismic deformation 1997-1999 191

5.5.4 Post-seismic deformation 2001-2002 191

5.6 Discussion 194

5.6.1 Aftershocks 195

5.6.2 Directivity 196

5.6.3 Afterslip 197

Electronic Appendix **201**

List of Figures

1 Three-dimensional perspective of Nazca subduction 2
2 Schematic illustration of volcanic deformation 3
3 Published GPS station locations 6
4 Cartoon of repeat-pass interferometry 7
5 Interferometry visual flow chart 8

1.1 Reference map of volcanoes in the central Andes 15
1.2 Interferometric coherence in the central Andes 18
1.3 Temporal coverage at volcanoes in the central Andes 21
1.4 Earthquake and volcanic deformation in the central Andes 24
1.5 Co-eruptive interferograms at Sabancaya 31
1.6 Lack of deformation at Lascar and Chiliques 34
1.7 Sensitivity to volume change from spherical source 36
1.8 Hydrological deformation in southern Peru 43
1.9 Deformation of salars in the central Andes 44
1.10 Decorrelation of salars in the central Andes 45
1.11 Shallow earthquake in Chile 49
1.12 Unknown sources of deformation 52

2.1 Location of volcanic deformation centers 60
2.2 Effects of elastic structure 66
2.3 Deformation at Uturuncu volcano 69
2.4 Scatter plots of source parameters 71
2.5 Trade-off between depth and volume 72

2.6 Comparison of model fits for different geometries 75
2.7 Comparison of source depths at different volcanoes 76
2.8 Time variations of volume change 78
2.9 Deformation at Hualca Hualca volcano 81
2.10 Atmospheric contamination near Hualca Hualca 82
2.11 Residual anomaly at Hualca Hualca 83
2.12 Deformation at Lazufre 85
2.13 Deformation at Cerro Blanco caldera 87
2.14 Volcanic extrusions of volcanic arc for different timescales 94

3.1 Reference map for geodetic study of 1995 Antofagasta earthquake . . . 102
3.2 Historic earthquake ruptures in northern Chile 104
3.3 Effect of missing lines upon phase 107
3.4 Possible ionospheric effects in interferogram 109
3.5 InSAR data used to study 1995 Antofagasta earthquake 110
3.6 Comparison of fit to InSAR data at different resolutions 112
3.7 Cross section through 1995 Antofagasta earthquake rupture area . . . 114
3.8 Comparison of model resolution from different inversion techniques . . 115
3.9 Residual as a function of singular values 118
3.10 Slip vectors of 1995 Antofagasta earthquake 119
3.11 InSAR residual from preferred model 120
3.12 GPS residual from preferred model 121
3.13 Comparison of model resolution from different datasets 125
3.14 Comparison of InSAR and GPS measurements 127
3.15 Comparison of model and coralline algae uplift 128
3.16 Wrapped InSAR displacements from previous inversions 130
3.17 Unwrapped InSAR displacements from previous inversions 131

4.1 Recent large earthquakes in northern Chile 136
4.2 Interferograms of recent large earthquakes in northern Chile 138
4.3 Seismograms for the 1998 earthquake 141

4.4 Seismograms for the 1995 earthquake 142
4.5 Comparision of slip inversions for the 1998 earthquake 148
4.6 InSAR residual for the 1998 earthquake 149
4.7 Comparision of slip inversions for the 1995 earthquake 152
4.8 InSAR residual for the 1995 earthquake 153
4.9 Small, deep earthquakes in northern Chile 155
4.10 Travel time relocation for the 1987 earthquake 157
4.11 Earthquake relocations 159
4.12 Predicted GPS displacements from post-seismic fluid flow 162
4.13 GPS post-seismic displacements 164
4.14 First year InSAR post-seismic deformation 165
4.15 Published GPS displacements 166
4.16 Post-seismic interferograms 1995-2000 169
4.17 Slip on the northern Chile subduction interface 1987-2000 172

5.1 Interferograms of large subduction zone earthquakes 178
5.2 Historic earthquake ruptures in southern Peru 179
5.3 ERS and JERS data for the 1996 Peru earthquake 182
5.4 InSAR data and residuals for the 2001 Peru earthquake 184
5.5 Deformation from the 2001 earthquake at the Arequipa GPS station . 185
5.6 Comparison of slip from the large Peru and Chile earthquakes 188
5.7 InSAR residuals for the 1996 Peru earthquake 189
5.8 Post-seismic interferograms for the 1996 Peru earthquake 192
5.9 Post-seismic interferogram for the 2001 Peru earthquake 193

List of Tables

1.1 Volcanoes surveyed in the central Andes 19

2.1 InSAR data used at actively deforming volcanoes 68
2.2 Source parameters for different geometries 74

3.1 InSAR data used in geodetic study of Antofagasta earthquake 108

4.1 InSAR observations in northern Chile 140
4.2 Recent post-seismic deformation at subduction zones 174

5.1 InSAR data for Peru earthquakes 181

Overview

0.1 Introduction to subduction zones

Subduction zones are of fundamental importance to planetary evolution, and the process of subduction is dynamic, generating mountain ranges, volcanoes, and the largest earthquakes (e.g., *Stern*, 2002). In this thesis, I use observations of recent crustal deformation to constrain sub-surface processes associated with several subduction zone earthquakes and volcanoes in west-central South American (14-28°S, see Figure 1) during the past 10 years.

In Chapters 1 and 2, I focus on deformation in the volcanic arc to determine which of the nearly one thousand volcanoes are actively deforming and might over lie regions where magma is moving at depth (see Figure 2). Once deformation is detected, it is difficult to determine the cause and potential hazard of eruption, because deformation can be caused by many processes (e.g., melting, magma injection, or ground water movements). I constrain the location and temporal evolution of the deformation sources, and this provides some clues as to the magma storage and plumbing system as well as the cause of the deformation. I then use these observations to estimate the mass moving within the arc over the past ten years (both intruded shallowly and extruded), and compare it with geologic estimates of the rate of magmatic addition.

In Chapters 3-5, I document the deformation associated with the subduction zone earthquake cycle for several large shallow thrust earthquakes in southern Peru and northern Chile. The classic model of the subduction zone earthquake cycle assumes that on timescales comparable to the earthquake cycle, co-seismic deformation exactly balances the post-seismic and inter-seismic deformation, resulting in no net deforma-

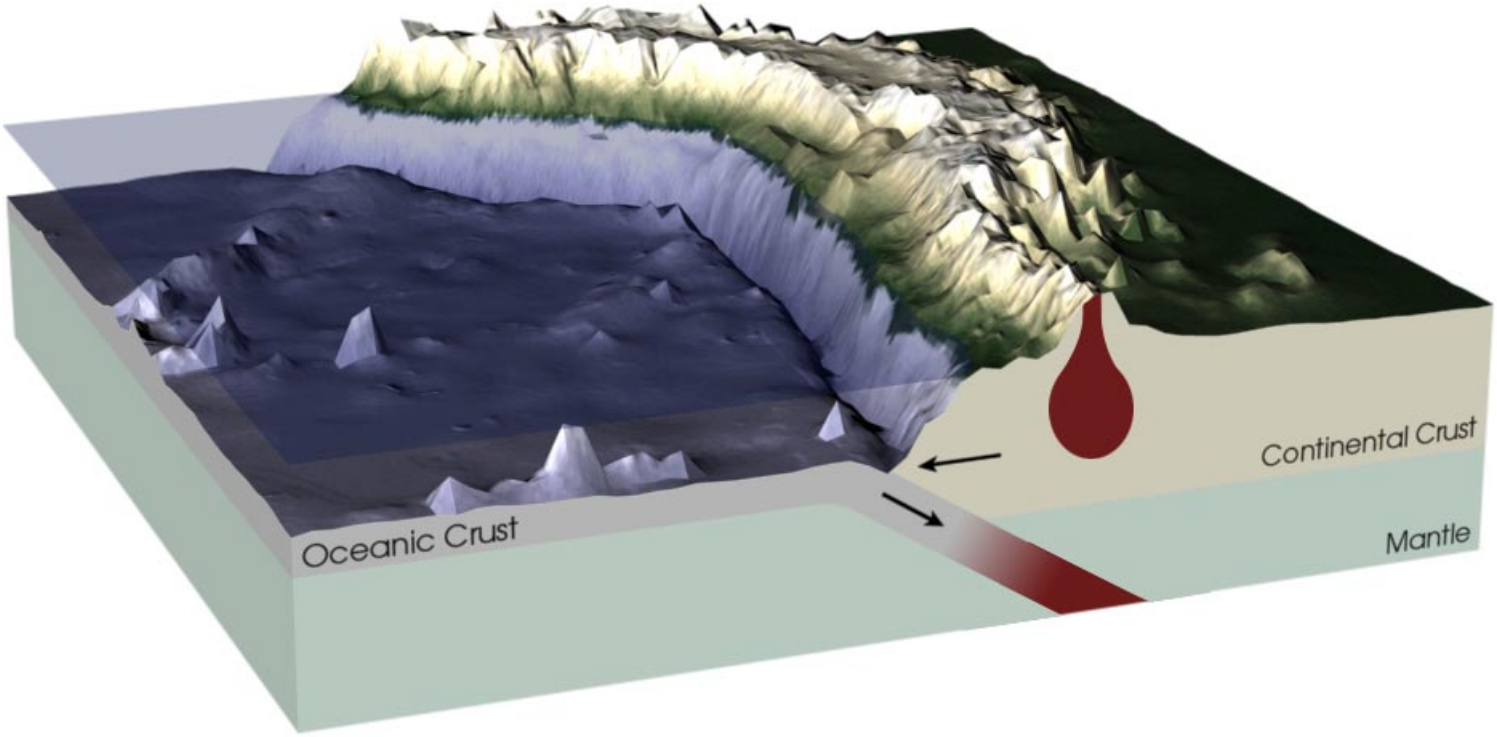

Figure 1: Three-dimensional cut-away perspective of the subduction of the Nazca plate beneath South America within the study area of this thesis, showing the bathymetry, topography, crustal structure and magmatism of the volcanic arc. (Image created by Robert Simmon, Goddard Space Flight Center.)

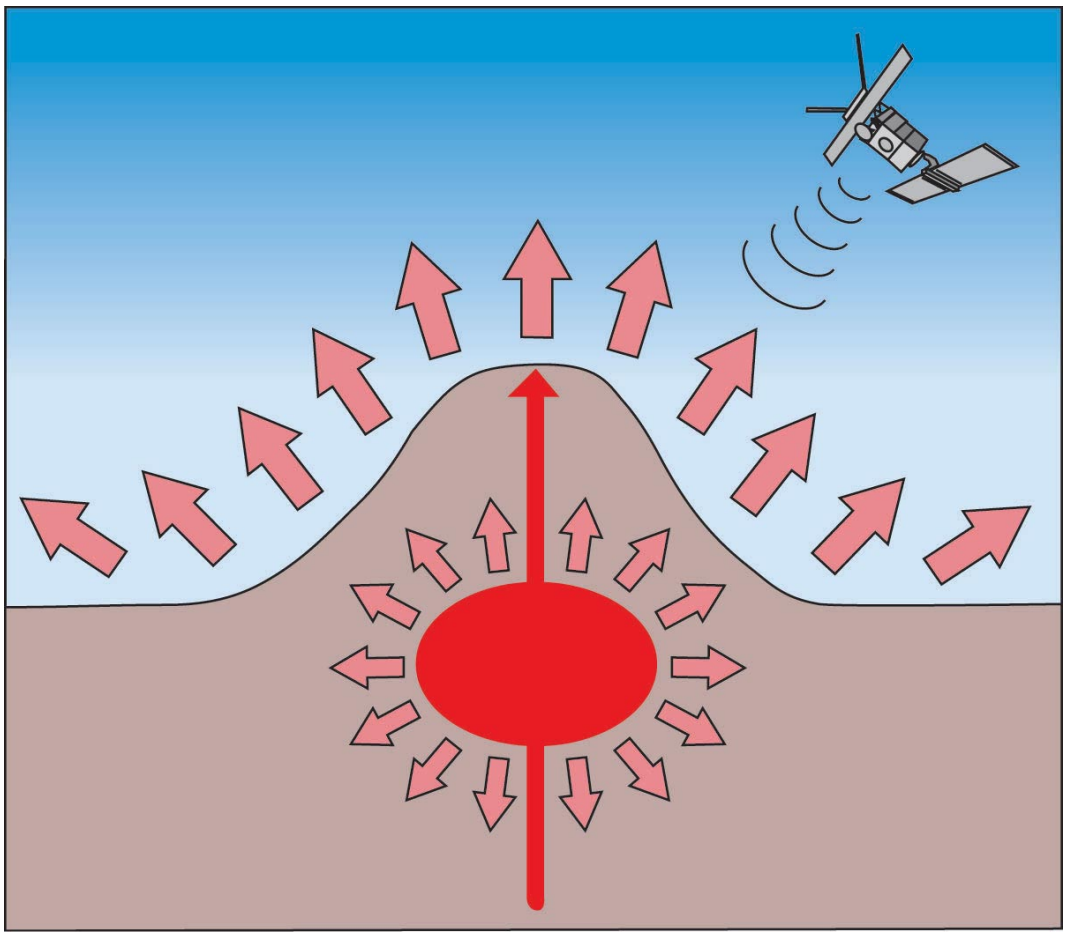

Figure 2: Schematic illustration of magma filling a magma chamber and causing surface inflation that is measured by an overflying radar satellite. (Image created by Doug Cummings, Caltech Public Relations.)

tion (*Savage*, 1983). While this might be a good approximation in some locations, in others, there is evidence for long-term coastal uplift or subsidence, indicating that over the earthquake cycle uplift and subsidence do not cancel (e.g., *Sato and Matsu'ura*, 1992; *Hsu*, 1992; *Delouis et al.*, 1998).

To better understand the long-term deformation at subduction zones, detailed spatial-temporal measurements of deformation are needed to constrain the variations in co-seismic and post-seismic deformation along strike. I find that even within this single subduction zone, there are significant differences in the earthquake cycle along strike over decadal timescales. In particular, the amount of deformation in the weeks to months following the 2001 M_w 8.4 Arequipa, Peru, was much greater than the deformation in the same time interval following the 1995 M_w 8.1 Antofagasta, Chile, earthquake, 300 km to the south. While these measurements only constrain deformation over the past few years, and not over the entire earthquake cycle (lasting hundreds of years), the along strike variations in the earthquake cycle documented in Chapter 5 provide some clues for understanding the mechanisms that control post-seismic deformation (particularly afterslip).

0.2 Introduction to radar interferometry

To measure surface deformation over the large areas spanned by the volcanic arc and the large subduction zone earthquakes, my primary tool is spacebourne interferometric synthetic aperture radar (InSAR). I also use seismic and Global Positioning System (GPS) observations to constrain slip on the subduction zone interface (Chapters 3-5). InSAR is a technique for atmospheric monitoring, and measuring topography and surface deformation that has been used for more than a decade (for a complete history, see *Rosen et al.*, 2000). InSAR is capable of measuring deformation of the Earth's surface with a pixel spacing of order ten meters over hundreds of kilometers, with an accuracy of better than one centimeter. Several publications have thoroughly outlined the technical principles of Synthetic Aperture Radar (SAR) (e.g., *Curlander and McDonough*, 1991; *Price*, 1999) and InSAR (e.g., *Griffiths*, 1995; *Gens and van*

Genderen, 1996; *Massonnet and Feigl*, 1998; *Rosen et al.*, 2000; *Bürgmann et al.*, 2000; *Wright*, 2000; *Hanssen*, 2001).

For the detailed studies of fault slip and the location of volcanic deformation in this thesis, the high spatial resolution and large lateral coverage of InSAR is essential. GPS is a proven technology for measuring crustal deformation (e.g., *Segall and Davis*, 1997), but although there are several GPS arrays in South America (Figure 3), including hundreds of stations, the station spacing is rather coarse. For example, there are only 3 and 14 GPS measurements of co-seismic deformation from the 1996 and 2001 Peru earthquakes, respectively (both with rupture lengths > 100 km) (*Norabuena et al.*, 2001), and only 16 measurements of post-seismic deformation from the 1995 Chile earthquake (*Klotz et al.*, 2001). Measurable deformation for all of these events spans hundreds of km^2. In Chapters 4 and 5, we present of order 10^8 InSAR observations of deformation for the same events. Of course, where possible, data from InSAR and GPS are combined, as the two datasets are complementary (see Chapters 3 and 5).

An illustration of the important interferometry steps is given in Figure 4 and 5. Radar energy is transmitted and received during a satellite (or aircraft) pass (Figure 4). The radar returns are then processed into images with both a magnitude (Figure 5, top row) and phase (Figure 5, second row) of the radar pulse for each pixel. The magnitude forms a recognizable image, in this case of Long Valley caldera, California, where the black area is Lake Crowley. The phase in a single radar image is a complex function of the ground surface scatterers (trees, mountains, people, etc.) resulting in an image that looks like white noise, with values distributed between 0 and 2π radians. However, when the phase from the two images is combined in an interferogram (lower right), the phase difference varies in a coherent manner. Several factors influence the phase (Figure 4) – satellite geometry, topography and surface deformation. Atmospheric contamination can also affect the phase measurements, which I discuss in Chapter 2. In this example, the effects of satellite geometry has been removed, so the image only includes topography and the interferogram resembles a topographic contour map (Figure 5, bottom right). Interferograms such as these

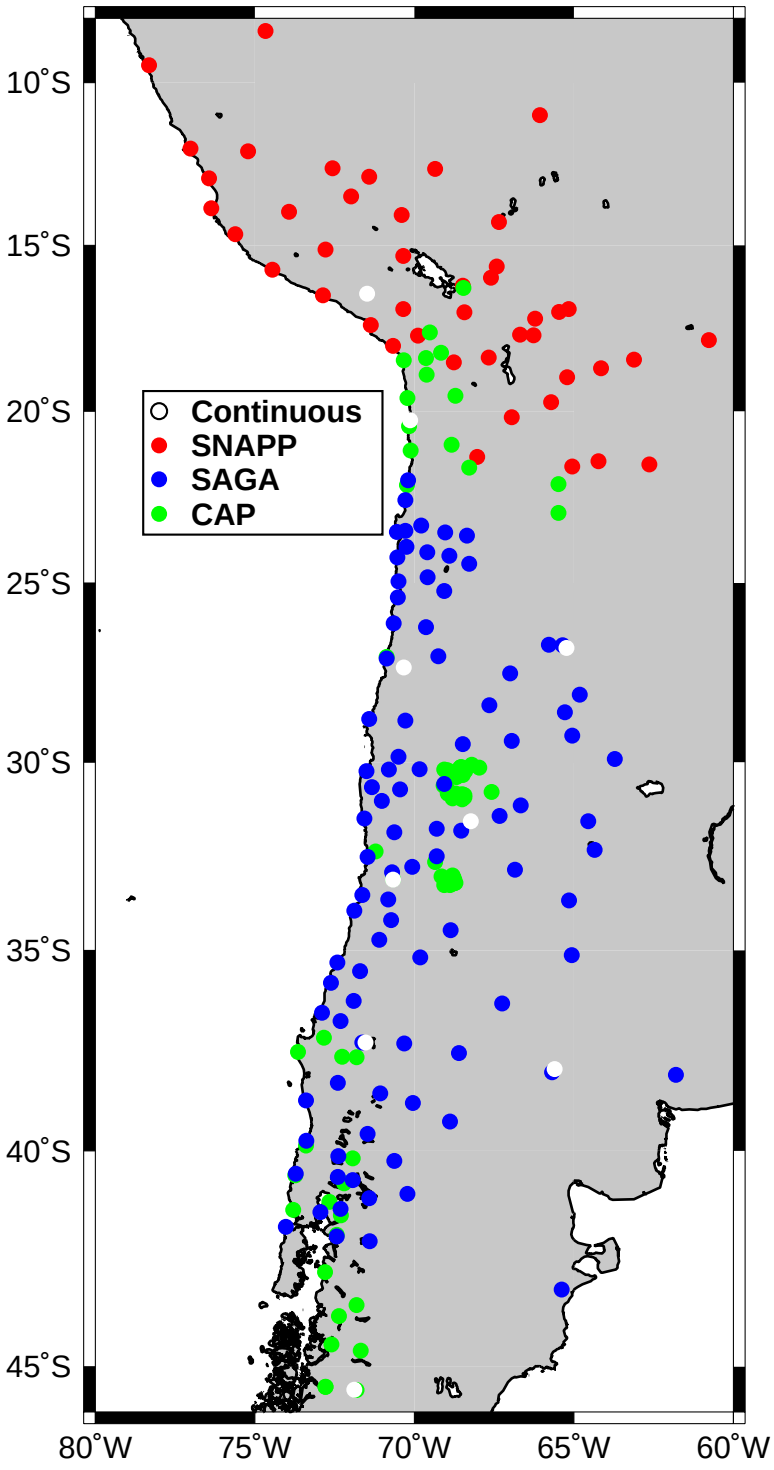

Figure 3: Published locations of GPS stations – Other monuments and continuous stations exist, but their locations are not publically available. Each circle represents a different benchmark, with red from SNAPP (*Norabuena et al.*, 1998), green from CAP (*Kendrick et al.*, 2001); blue from SAGA (*Klotz et al.*, 2001), and white corresponding to continuous GPS stations (the others are all campaign) run by IGS and CAP (*Kendrick et al.*, 1999).

can be used to generate digital elevation models (DEM) of an area, and for my thesis and other projects, I have used interferograms to create DEM's in several areas of South America. To measure surface deformation, we must remove the effects of the topography from the interferogram, either by using a pre-existing DEM (the so-called 2-pass approach), or by using an interferogram that is known to include only topography and not deformation (the 3- or 4-pass approach). All of these methods were used in this thesis.

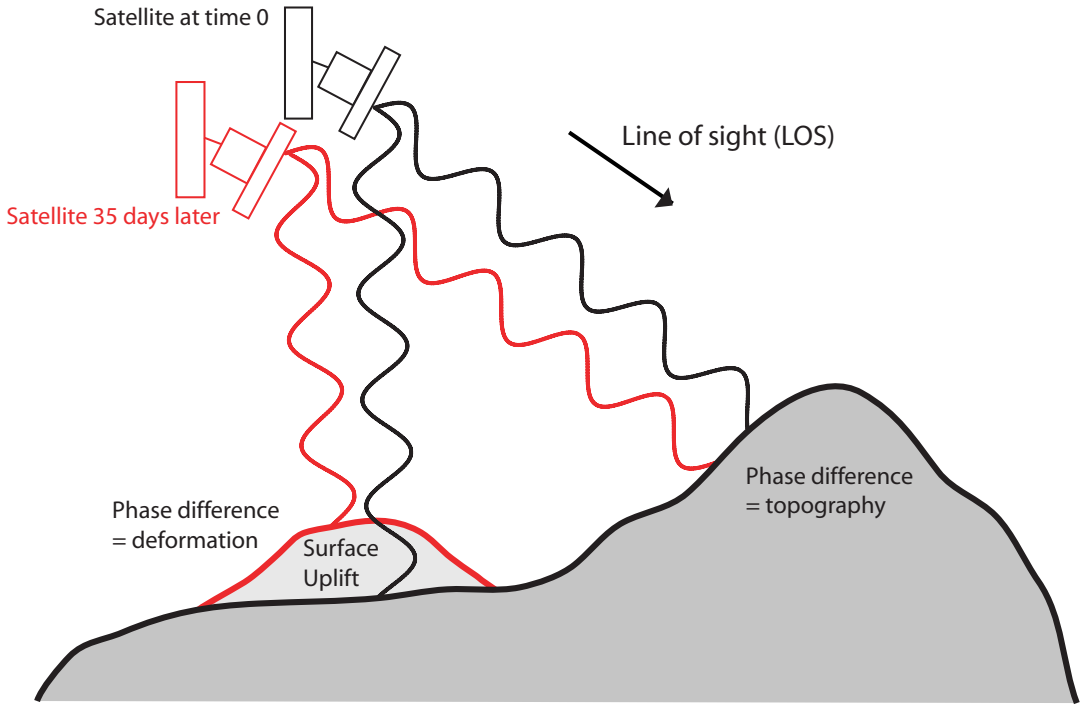

Figure 4: Repeat pass interferometry: During an initial pass over an area, a radar satellite sends an electromagnetic beam to the ground (black lines) and repeats the same operation at a later time from a slightly different perspective (red lines). The red and black wavelengths are out of phase because of the different viewing angles (which is particularly pronounced over topography – the parallax effect, see right side of Figure), and because of surface deformation on the left-hand side of the image.

In terms of measuring surface deformation, the satellite InSAR observations are only sensitive to the line of sight (LOS) component. For an individual interferogram, this means that only one-component of the deformation field can be measured.

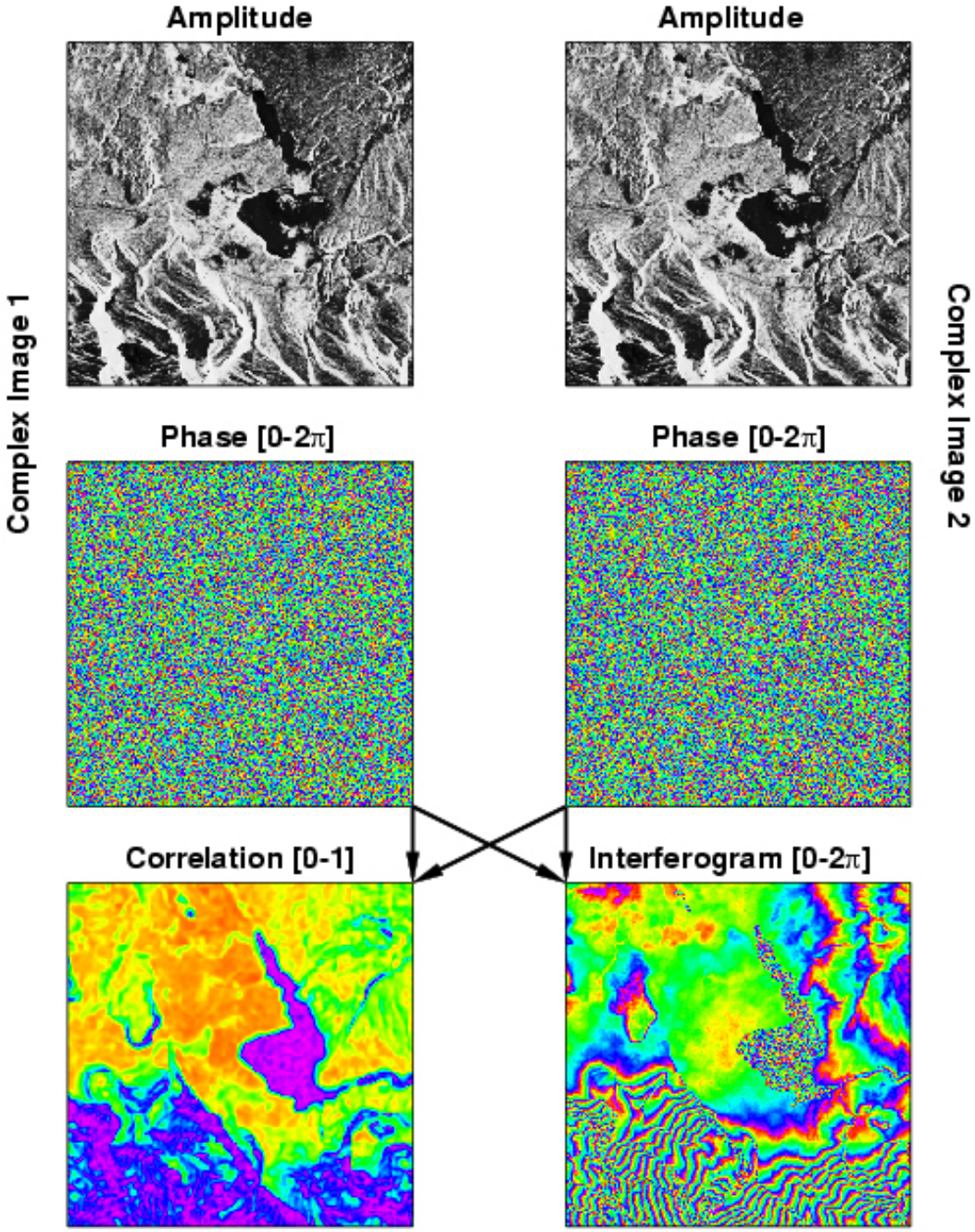

Figure 5: Interferometry flow chart: SAR amplitude (top row) and phase (second row) images of Lake Crowley in Long Valley, California, are used to form an interferogram (lower right) and coherence map (lower left). See text for details. (Image created by Mark Simons).

Multiple satellite passes with different observation geometries can be used to recover more than one component of deformation (Chapters 2 and 3), and if enough data is available, the 3-D deformation field can be reconstructed (e.g., *Fialko et al.*, 2001b).

In some regions, the procedure for creating an interferogram fails – the phase is not coherent during the time interval because the radar scattering properties of the ground changed. A map of the coherence is shown in Figure 5 (lower left) where purple colors indicate low coherence and red colors correspond to areas of high coherence. Lake Crowley is uncorrelated because the scattering properties of water surfaces at the scale of the radar wavelength change completely between observations.

I use the InSAR processing software called ROI_PAC (Repeat Orbit Interferometry PACkage), developed at the Jet Propulsion Laboratory and Caltech. This package allows both experienced and new users to processes raw SAR data into a final product that is unwrapped and geolocated and ready for geophysical modeling. Using this software, I have processed about 400 scenes of SAR data from South America for this thesis. The software source code is freely available at the website http://www.openchannelfoundation.org/projects/ROI_PAC/. During the course of this thesis, I have assisted in the development of ROI_PAC by writing new programs, modifying existing programs and scripts, and discussing problems and suggestions with the other developers. I discuss some of the specific technical issues that had to be corrected in order to complete this thesis in Chapters 1-3. Details of the software implementation have been published by *Buckley* (2000), and practical suggestions by *Schmidt* (2002).

0.3 Thesis outline

While this thesis is united by a common tool (InSAR) and study area (west-central South America), each chapter is relatively independent. Chapter 1 documents our survey for volcanic deformation in the central Andes, and provides details on the data used, our sensitivity to deformation, and the volcanic and non-volcanic sources of deformation. Four volcanoes erupted in this area during our period of observation,

and we document the lack of deformation associated with any of these eruptions, and give possible explanations for the lack of deformation. In addition, Chapter 1 documents our field visits to several of the volcanoes.

In Chapter 2, we model the four sources of volcanic deformation documented in Chapter 1. We can explain the observed deformation with a variety of models, including centers of deformation that are spherical, prolate or oblate. Based on the depth of the sources, we think that three of the deformation sources are related to magmatism. The amount of deformation at the fourth source (an area of subsidence) can not be explained simply by conductive cooling, so we infer the existence of a hydrothermal system. We compare the amount of material erupted in the central Andes between 1992-2002 with the volume of magma we infer to be moving at depth, and find a ratio of intrusion/extrusion between 1-10. The rate of magmatic addition to the arc over the ten year period is similar to geologic averages for the central Andes and other volcanic arcs.

The focus moves to earthquakes in Chapter 3, where we constrain the fault slip from the 1995 M_w 8.1 Antofagasta, Chile, earthquake with InSAR and GPS. We test the ability of the different datasets to resolve slip along the fault interface for this earthquake, and two different inversion methods for calculating fault slip. We find that previous fault slip models made by inverting seismic and sparse GPS observations are inconsistent with the InSAR observations.

We continue our study of subduction zone earthquakes in northern Chile in Chapter 4. We use InSAR and seismic data to invert for fault slip from the 1995 M_w 8.1 and 1998 M_w 7.1 Antofagasta, Chile, earthquakes. We use seismic data to relocate three $M_w > 7$ earthquakes from the 1980's. We find that the rupture areas of the five earthquakes do not overlap. The 1995 event did not rupture to the bottom of the seismogenic zone, whereas the earthquakes in 1998 and 1987 did. Using InSAR and GPS, we constrain the moment of the post-seismic deformation following the 1995 earthquake to be about 5% of the co-seismic moment, which is anomalously low compared to other subduction zone earthquakes.

In Chapter 5, we use InSAR and GPS to study the co-seismic and post-seismic

deformation from two large subduction zone earthquakes in southern Peru: 1996 M_w 7.7 Nazca, Peru; and 2001 M_w 8.4 Arequipa, Peru. We infer that both of these events ruptured to the bottom of the seismogenic zone. While we do not observe any post-seismic deformation from the 1996 event, there is significant deformation following the Arequipa earthquake recorded by GPS. We compare and contrast the co-seismic and post-seismic deformation from the 1995, 1996 and 2001 earthquakes.